from the flammability regime, residence times are very short, and catalyst walls inhibit gas-phase free-radical chain reactions.

The proposed mechanism of catalytic CH_4 pyrolysis followed by H_2 desorption and carbon oxidation appears to explain the high selectivity of syngas formation very well by using elementary steps from the surface science literature. The large differences between Pt and Rh also correlate well with their adsorption, desorption, and reaction properties. The ability to utilize models of catalytic processes such as these will be crucial in designing catalytic combustors and reactors for pollution control and efficient synthesis of chemicals with catalytic processes.

REFERENCES AND NOTES

1. C. N. Satterfield, *Heterogeneous Catalysis in Practice* (McGraw-Hill, New York, ed. 2, 1991).
2. S. J. Conway, D. J. Wang, J. H. Lunsford, *Appl. Catal. A: Gen.* **79**, L1 (1991).
3. J. C. Mackie, *Catal. Rev. Sci. Eng.* **33**, 169 (1991).
4. J. D. Korchnak, M. Dunster, A. English, *World Intellectual Property Organization Reports WO 90/06282 and WO 90/06297* (Geneva, 1990).
5. R. F. Blanks, T. S. Wittrig, D. A. Peterson, *Chem. Eng. Sci.* **45**, 2407 (1990).
6. D. Dissanayake, M. P. Rosynek, K. C. C. Kharas, J. H. Lunsford, *J. Catal.* **132**, 117 (1991).
7. A. T. Ashcroft *et al.*, *Nature* **344**, 319 (1990).
8. P. D. F. Vernon, M. L. H. Green, A. K. Cheetham, A. T. Ashcroft, *Catal. Lett.* **6**, 181 (1990).
9. J. K. Hochmuth, *Appl. Catal. B: Env.* **1**, 89 (1992).
10. A. B. Anderson and J. J. Maloney, *J. Phys. Chem.* **92**, 809 (1988).
11. W. R. Williams, C. M. Marks, L. D. Schmidt, *ibid.* **96**, 5922 (1992).
12. G. B. Fisher and J. L. Gland, *Surf. Sci.* **94**, 446 (1977).
13. R. W. McCabe and L. D. Schmidt, *ibid.* **65**, 189 (1977).
14. T. Matsushima, *ibid.* **157**, 297 (1985).
15. C. T. Campbell, G. Ertl, H. Kuipers, J. Segner, *J. Chem. Phys.* **73**, 5862 (1980).
16. ———, *Surf. Sci.* **107**, 207 (1981).
17. S. G. Brass and G. Ehrlich, *J. Chem. Phys.* **87**, 4285 (1987).
18. M. L. Wagner and L. D. Schmidt, *J. Phys. Chem.*, in press.
19. M. P. Zum Mallen, W. R. Williams, L. D. Schmidt, *ibid.*, in press.
20. J. T. Yates, P. A. Thiel, W. H. Weinberg, *Surf. Sci.* **82**, 45 (1979).
21. S. H. Oh, G. B. Fisher, J. E Carpenter, D. W. Goodman, *J. Catal.* **100**, 360 (1986).
22. T. W. Root, L. D. Schmidt, G. B. Fisher, *Surf. Sci.* **134**, 30 (1983).
23. J. Kiss and F. Solymosi, *ibid.* **177**, 191 (1986).
24. F. T. Wagner and T. E. Moylan, *ibid.* **191**, 121 (1987).
25. L. S. Brown and S. J. Sibener, *J. Chem. Phys.* **89**, 1163 (1988).
26. C. T. Campbell, S.-K. Shi, J. M. White, *J. Phys. Chem.* **83**, 2255 (1979).
27. P. A. Thiel, E. D. Williams, J. T. Yates, Jr., W. H. Weinberg, *Surf. Sci.* **84**, 54 (1979).

28. Supported in part by DOE grant DE-FG02-88ER13878-A02.

9 September 1992; accepted 24 November 1992

Single Crystal Metals Encapsulated in Carbon Nanoparticles

Rodney S. Ruoff, Donald C. Lorents, Bryan Chan, Ripudaman Malhotra, Shekhar Subramoney

Single-domain microcrystals of LaC_2 encapsulated within nanoscale polyhedral carbon particles have been synthesized in a carbon arc. Typical particle sizes are on the order of 20 to 40 nanometers. The stoichiometry and phase of the La-containing crystals have been assigned from characteristic lattice spacings observed by high-resolution transmission electron microscopy and energy dispersive spectroscopy (EDS). EDS spectra show that La and C are the only elements present. Characteristic interatomic distances of 3.39 and 2.78 angstroms identify the compound inside the nanoparticle cavities as α-LaC_2, the phase of LaC_2 that is stable at room temperature. Bulk α-LaC_2 is metallic and hydrolytic. Observation of crystals of pure encapsulated α-LaC_2 that were exposed to air for several days before analysis indicates that the LaC_2 is protected from degradation by the carbon polyhedral shells of the nanoparticles. A high percentage of the carbon nanoparticles have encapsulated LaC_2 single crystals. These carbon-coated metal crystals form a new class of materials that can be protected in their pure or carbide forms and may have interesting and useful properties.

The nested carbon nanotubes discovered by Iijima (*1*, *2*) as a by-product of fullerene production have extended the dimensions and geometries of fullerenes into the domain of nanoparticles. Interest in the unique electrical and thermal properties of these structures has resulted from several theoretical calculations which suggest that the structures have metallic or semiconductor properties (*3*–*7*). The discovery of a means for enhanced production of the tubes reported by Ebbeson and Ajayan (*8*) suggests that sufficient quantities of these particles can be made to permit their properties to be measured.

We have found that the tubes are produced together with a large variety of polyhedral carbon nanoparticles that frequently contain internal cavities. A typical transmission electron microscopy (TEM) scan of material obtained from the core of a growth on a carbon electrode in an arc discharge in 500 torr of He (Fig. 1) shows an assembly of tubules together with a variety of nanodimension carbon particles that are evidently polyhedral shells. The particles consist of several nested layers of carbon enclosing internal cavities of various sizes. They can be considered to be super-giant nested fullerenes with their polyhedral geometries defined by the placement of 12 pentagons in a hexagon lattice. We report here the successful filling of these cavities with metals. We find that the carbon arc conditions which favor nanotube and nanoparticle growth can be exploited to completely encapsulate metals.

In analogy with the production of endohedral fullerenes, our first attempt to fill the cavities of these carbon nanoparticles made use of a graphite rod packed with an electropositive metal. The successful production of La endohedral fullerenes (*9*–*12*) suggested that La was a good candidate for incorporation into the nanoparticles. The 7.9-mm-diameter, 30.5-cm-long graphite positive electrode was drilled to a depth of 23 mm with a 3.2-mm drill and packed with La_2O_3. The rod, which was weighed before and after packing with La_2O_3, provided an La:C molar ratio of 0.02. The carbon arc conditions included a DC current of 150 A, a gap distance of about 1 mm between the stationary 12.7-mm-diameter negative electrode and the translating positive electrode, and an He pressure of 500 torr.

The deposited cylindrical growth on the end of the negative electrode was substantially more fragile than growths obtained without the La present. Extracting the central core was therefore difficult, and the cylinder often crumbled. The powder obtained was dispersed in ethanol by using an ultrasonic bath and deposited on carbon-coated grids for TEM studies. Conventional bright-field and high-resolution lattice fringe images were obtained with a JEOL 2000-FX TEM operated at 200 kV. Elemental analysis was performed with a high-angle Noran energy dispersive spectroscopy (EDS) analyzer with a Be window and Ge detector. For specific identification of the composition of low Z materials in the carbon nanoparticles, a Phillips CM-30 TEM equipped with a windowless Link EDS analyzer was used.

Figure 2 shows an example of a nanoparticle enclosing what appears to be a single crystal, as evidenced by its regular set of lattice fringes. The crystal boundaries conform to the interior carbon shell walls, which suggests that the particle is completely enclosed within the carbon nanoparticle. An EDS spectrum from the JEOL 2000-FX

R. S. Ruoff, D. C. Lorents, B. Chan, R. Malhotra, Molecular Physics Laboratory, SRI International, Menlo Park, CA 94025.
S. Subramoney, Du Pont Company Experimental Station, Wilmington, DE 19880–0228.

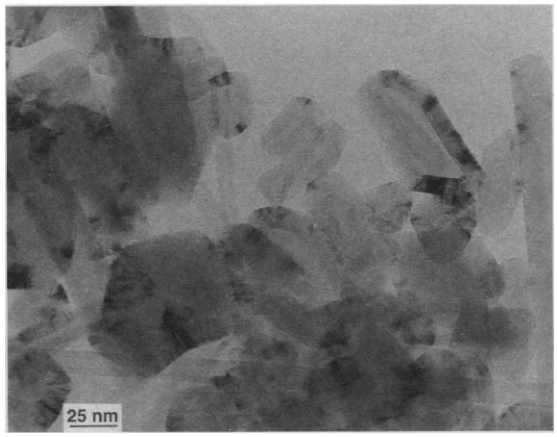

Fig. 1. Bright-field TEM micrograph of material from a standard arc-discharge experiment. Several carbon nanoparticles that vary in size from 20 to 40 nm and that have empty internal cavities are present.

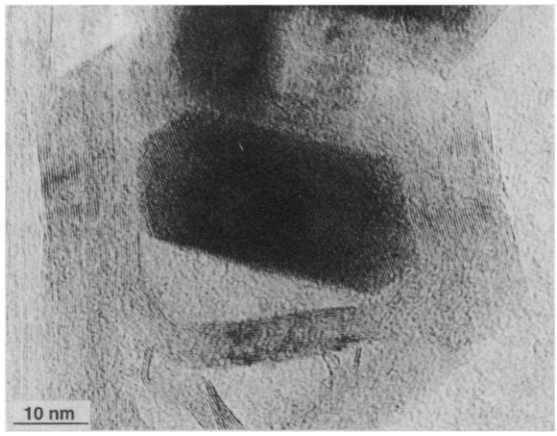

Fig. 2. High-resolution TEM image of a single crystal of LaC_2 that is encapsulated inside a carbon nanoparticle. There are about 30 carbon shells, and the layer spacing between them is 3.42 Å. The fringe spacing between the planes in the LaC_2 is 3.39 Å, which corresponds to the spacing in the (101) plane of α-LaC_2. The α-LaC_2 partially fills the available volume of the cavity.

exhibited the characteristic peaks associated with La, and an EDS spectrum obtained with the windowless detector clearly showed the presence of only carbon and La; no characteristic peaks of oxygen were evident. La_2O_3 was run as a standard, and the observed O/La peak ratios in the EDS spectrum of this standard indicated that the O content of the La/C sample was extremely low. Therefore, La and C are the only elements present in significant quantities. Low-resolution TEM scans (not shown) indicated that a large fraction of the carbon nanoparticles have encapsulated metal crystals. A rough estimate, obtained from a statistical survey of several TEM micrographs, is that 50% of the nanoparticles contain encapsulated metal crystals.

The phase diagram of carbides of La is well characterized and shows several possibilities for the encapsulated crystals, including La, La_3C, La_2C_3, and LaC_2 (*13*). The known characteristic lattice (*d*) spacings for the different phases of each of these compounds permit the unambiguous identification of the encapsulated material. Two distinct *d* spacings are observed in these crystals; the ratio of these spacings, which is independent of any calibration standard, is 1.22. Using the TEM calibration marker, we obtain *d* spacings of 3.39 and 2.78 Å. The same TEM standard gives 3.42 Å for the carbon lattice spacing, in agreement with Iijima (*1*). Only α-LaC_2 has lattice spacings matching the observed ratio and absolute *d* values. The reported *d* values obtained by x-ray diffraction measurements of α-LaC_2 are 3.375 and 2.782 Å, respectively (*14*).

Thus, the encaged crystals are clearly identified as α-LaC_2, which is consistent with the phase diagram under the carbon-rich conditions of growth in this case. It is possible that some of the crystals are La_2C_3, which has one *d* spacing (namely, the 2.78 Å spacing) that matches one of the observed spacings. However, two other resolvable characteristic *d* spacings of La_2C_3, 3.58 and 3.11 Å, were not observed in any of 15 encapsulated crystals surveyed with quality fringe patterns. The absence of these spacings in our survey of TEM micrographs suggests that α-LaC_2, the phase richest in carbon, is the only carbide of La present. This was independently confirmed by x-ray-diffraction (XRD) of the sample powder. Four characteristic *d* spacings of α-LaC_2 were observed, with the literature values (*14*) in parentheses: 2.800 Å (2.782), 2.136(2.123), 1.980(1.967), and 1.925 (1.914). The high intensity (211) and (220) peaks of La_2C_3 (*15*) corresponding to d = 3.58 and 3.11 Å, respectively, and which would appear without overlap in the powder XRD of the sample, were absent.

α-LaC_2 has the crystal structure of CaC_2 and is the room-temperature-stable phase of LaC_2 (*13*). The transition temperature between the high-temperature β-LaC_2, which crystallizes with the CaF_2 structure (bcc fluorite), and the low-temperature α-LaC_2 phase is 1060°C (*16*). The β-LaC_2 phase is 6.7% less dense than the α-LaC_2 phase (*17*). LaC_2, like CaC_2, rapidly undergoes hydrolysis. The products are La_2O_3 and primarily acetylene (with minor amounts of other hydrocarbons) (*14*). The samples we examined by TEM had been exposed to air for several days prior to analysis and showed no evident degradation, which suggests that they are protected by the multilayered carbon nanoparticle cage.

In contrast to CaC_2, α-LaC_2 is a metal (*18*). The reason α-LaC_2 is a metal is that La is present in the oxidation state +3 and C_2 is present in the -2 state; thus, the C_2 contributes the extra electron to the conduction band. The conductivity of α-LaC_2 at 273 K is about 3600 times lower than that of copper (*19*). All of the enclosed La we observed was in the form of single α-LaC_2 crystals, and no evidence of amorphous compounds was found.

To summarize, single-domain α-LaC_2 nanocrystals have been encapsulated inside carbon nanopolyhedra. Synthesis is achieved in a DC carbon arc with La_2O_3 packed into the positive electrode at a 0.02 La:C ratio. This demonstration of the nanoscale encapsulation of metal crystallites within a protective carbon cage can perhaps be extended to many other materials and permit the utilization of a wide range of air-sensitive materials for applications not previously possible. It remains to investigate encapsulation of other metals and understand the growth process of these remarkable materials.

Note added in proof: Shortly before acceptance of this paper, the authors received a preprint from M. Tomita, Y. Saito, and T. Hayashi describing observation of LaC_2 encapsulation.

REFERENCES AND NOTES

1. S. Iijima, *Nature* **354**, 56 (1991).
2. _____, T. Ichihashi, Y. Ando, *ibid.* **356**, 776 (1992).
3. J. W. Mintmire, B. I. Dunlap, C. T. White, *Phys. Rev. Lett.* **68**, 632 (1992).
4. N. Hamada *et al.*, *ibid.*, p. 1579.
5. R. Saito, M. Fujita, G. Dresselhaus, M. S. Dresselhaus, *Phys. Rev. B* **46**, 1804 (1992).
6. J. W. Mintmire *et al.*, in *Electrical, Optical, and Magnetic Properties of Organic Solid State Materials*, L. Y. Chiang, A. F. Garito, D. J. Sandman, Eds., MRS Symposia Proceedings No. 247 (Materials Research Society, Pittsburgh, PA, 1992), p. 339.
7. K. Tanaka, K. Okahara, M. Okada, T. Yamabe, *Chem. Phys. Lett.* **191**, 469 (1992).

8. T. W. Ebbesen and P. M. Ajayan, *Nature* **358**, 220 (1992).
9. J. R. Heath *et al.*, *J. Am. Chem. Soc.* **107**, 7779 (1985).
10. Y. Chai *et al.*, *J. Phys. Chem.* **95**, 7564 (1991).
11. R. D. Johnson *et al.*, *Nature* **355**, 239 (1991).
12. L. Moro, R. S. Ruoff, D. C. Lorents, R. Malhotra, C. H. Becker, in preparation.
13. K. A. Gschneidner, Jr., and F. W. Calderwood, *Bull. Alloy Phase Diagr.* **7**, 446 (1986).
14. F. H. Spedding, K. A. Gschneidner, Jr., A. H. Daane, *J. Am. Chem. Soc.* **80**, 4499 (1958).
15. M. Atoji *et al.*, *ibid.*, p. 1804.
16. K. A. Gschneidner, Jr., and F. W. Calderwood, *Bull. Alloy Phase Diagr.* **7**, 421 (1986).
17. A. L. Bowman *et al.*, *Acta Crystallogr. Sect. B* **24**, 459 (1968).
18. T. Sakai, G. Adachi, T. Yoshida, J. Shiokawa, *J. Less-Common Metals* **81**, 91 (1981).
19. Table 3 of (*17*) quotes a value of 55.3 μΩ cm for the resistivity of α-LaC_2 at 273 K. The electrical resistivity of Cu at 273 K is 0.01543 μΩ cm [D. R. Lide, Ed., *Handbook of Chemistry and Physics*, ed. 73 (CRC Press, Ann Arbor, MI, 1992)].
20. The assistance of L. Hanna and E. Boyes of Du Pont Central Research and Development is deeply appreciated. Useful discussions with K. A. Gschneider, Jr., are also appreciated. Part of this work was conducted under the program "Advanced Chemical Processing Technology," which is consigned to the Advanced Chemical Processing Technology Research Association by the New Energy and Industrial Technology Development Organization and carried out under the Large-Scale Project administered by the Agency of Industrial Science and Technology, the Ministry of International Trade and Industry.

10 November 1992; accepted 17 December 1992

Paleohydrology of Late Pleistocene Superflooding, Altay Mountains, Siberia

Victor R. Baker,* Gerardo Benito,† Alexey N. Rudoy

Cataclysmic flooding is a geomorphological process of planetary significance. Landforms of flood origin resulted from late Pleistocene ice-dammed lake failures in the Altay Mountains of south-central Siberia. Peak paleoflows, which exceeded 18 × 10^6 cubic meters per second, are comparable to the largest known terrestrial discharges of freshwater and show a hydrological scaling relation to floods generated by catastrophic dam failures. These seem to have been Earth's greatest floods, based on a variety of reconstructed paleohydraulic parameters.

The long tradition in geomorphology of inferring cataclysmic flood origins for certain valley landforms (*1*) has produced incidents of less-than-critical hypothesizing of catastrophism (*2*), which has led to some scientific disrepute for such explanations (*3*). For the Channeled Scabland region of the northwestern United States (*4*), antiquated and outmoded concepts of uniformitarianism (*5*) hindered scientific recognition of pervasive field evidence that indicated that landscape's origin by cataclysmic flood processes (*6*). The mechanical processes associated with the Channeled Scabland flooding are now well established (*7*): the failure of ice-dammed Glacial Lake Missoula resulted in late Pleistocene peak discharges as great as 17 × 10^6 m^3 s^{-1} (*8*), and a distinctive suite of landforms (*9*) is associated with the immense stream power (*10*) expended by the Missoula flooding.

Cataclysmic flood processes similar to those responsible for the Channeled Scabland have been documented for late Pleistocene drainage of Lake Bonneville (*11*), for various spillways marginal to the Laurentide Ice Sheet (*12*), and for Swedish Lapland (*13*). More controversial are the cataclysmic glacial flood origins ascribed to submarine English Channel landforms (*14*) and to the extensive drumlin fields of North America (*15*). Landform assemblages characteristic of cataclysmic flooding have also been described on Mars (*16*). The Martian outflow channels are much larger than those of the Channeled Scabland and may have had discharges as great as 10^9 m^3 s^{-1} (*17*). Martian flooding occurred on such a grand scale that it probably would have affected global climate, thereby inducing a variety of climate-related geomorphological responses (*18*). Large-scale flood channels have also recently been found on Venus (*19*), though these floods probably involved highly fluid lavas that mimicked aqueous behavior (*20*).

Here, we describe cataclysmic flood features of the Altay Mountains of south-central Siberia (*21*). Many of these features were formerly ascribed to glaciation (*22*). However, they occurred in association with outflow routes from late Pleistocene ice-dammed lakes (Fig. 1). Landforms indicative of cataclysmic outburst floods from these lakes include flood-scoured channelways, giant bars, and gravel wave trains (Fig. 2).

For a reach of the Chuja River valley, immediately downstream of the Kuray Basin (Fig. 1), we estimated the mechanical processes responsible for these landforms. As

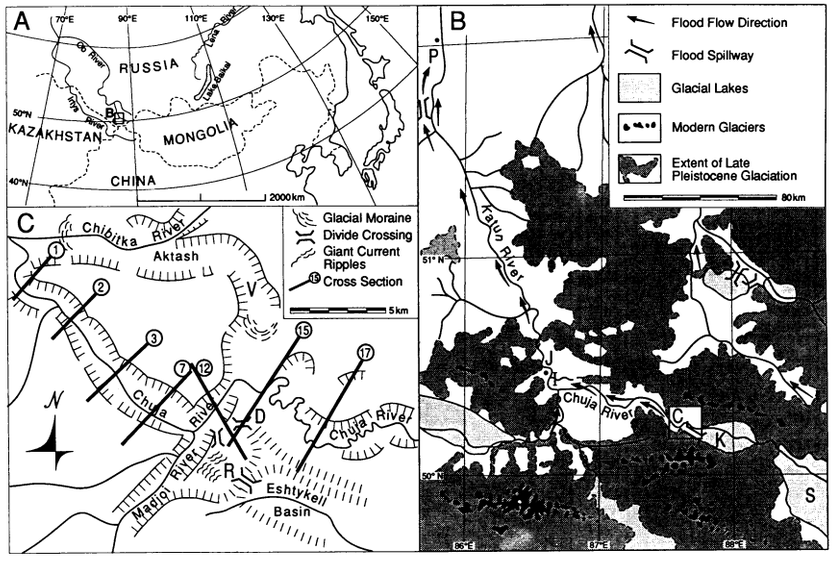

Fig. 1. (**A**) Location of Altay Mountain study site in the headwaters of the Ob River, Siberia. (**B**) Enlargement of box B in (A), showing the locations of late Pleistocene ice-dammed lakes of the Altay Mountains. K, Kuray Basin; S, Chuja Basin. Giant bars occur near Inya (I), and gravel wave trains occur at Little Jaloman (J) and Platovo (P). The reach chosen for hydraulic analysis (C) is located near the Kuray Basin ice dam. Late Pleistocene glacial and flood features are after Rudoy *et al.* (*27*). (**C**) Enlargement of box C in (B), showing details of the flood reach analyzed in Fig. 3 and locations of selected cross sections (numbered in the text and in Fig. 3). D, high-level divide crossing; R, gravel waves.

V. R. Baker and G. Benito, Arizona Laboratory for Paleohydrological and Hydroclimatological Analysis, Department of Geosciences, University of Arizona, Tucson, AZ 85721.
A. N. Rudoy, Geography Department, Tomsk State Pedagogical Institute, Tomsk, Siberia, Russia.

*To whom correspondence should be addressed.
†Present address: Centro de Ciencias Mediambientales, Consejo Superior de Investigaciones Cientificas, Serrano 115 dpdo, 28006 Madrid, Spain.